Underwater Technology 2000 conference
23-26 May 2000, Tokyo, Japan

SYSTEM IDENTIFICATION OF UNDERWATER VEHICLES

Javier Pereira and Alec Duncan

Australian Maritime Engineering CRC,
Curtin University of Technology,
Kent Street, Bentley, Western Australia, 6102.
E-mail: a.duncan@cmst.curtin.edu.au

Abstract - Unmanned underwater vehicles (UUV's) are used in a number of applications such as pipeline and offshore structure maintenance by the offshore oil industry, and for mine clearance by the navy. They typically operate in a large range of flow conditions making it difficult to predict the hydrodynamic forces acting on them, and consequently making vehicle control difficult.

The aim of this project was to obtain hydrodynamic derivative measurements from sea trials using an underwater vehicle which is a half-scale model of the PAP-104 mine countermeasures UUV. Trials data were collected for a series of manoeuvres which were then reconstructed to give the required vehicle state estimates. This reconstruction was carried out using an extended Kalman filter. Hydrodynamic derivative estimates were then generated by a stepwise regression algorithm, which took the reconstructed vehicle state and measured vehicle forces as input.

Traditionally these types of hydrodynamic measurements are made using a Planar Motion Mechanism (PMM). Any later changes to the vehicle configuration may reduce the usefulness of these measurements. Ideally system identification (SI) techniques would provide a more practical alternative, as the UUV need only be driven in a predefined way and the SI techniques applied in order to obtain current hydrodynamic measurements. SI techniques also give measurements based on the overall response of the vehicle and umbilical, which is not the case with PMM measurements.

Index terms - underwater vehicle, ROV, Kalman filter, system identification

I. INTRODUCTION

The half scale PAP-104 remotely operated underwater vehicle is essentially a rigid body with two fixed thrusters, one on either side. When in operation the ROV is connected to an umbilical (tether) as well as a chain. The umbilical serves as a communications link to the surface, while the chain is dragged along the seabed keeping the craft at an approximately constant depth.

This paper firstly outlines the hydrodynamic derivatives that were identified for the PAP 104, and the measurements taken during the sea trials. This is followed by a description of the extended Kalman filter used to estimate the vehicle state and some state estimation results from the trials. The paper finishes with the parameter estimation and some planar motion mechanism results for comparison.

II. HYDRODYNAMIC COEFFICIENTS

The coordinate system used to describe the vehicle motions is fixed to the vehicle with the positive *X* axis forwards, the positive *Y* axis to starboard and the positive *Z* axis downwards.

The forces acting on the underwater vehicle are described by Equation 1 [1]:

$$\underline{\underline{M}}\begin{bmatrix}\dot{u}\\ \dot{v}\\ \dot{w}\\ \dot{p}\\ \dot{q}\\ \dot{r}\end{bmatrix}=\begin{matrix}\underline{F}_d(u,v,w,p,q,r)+\\ \underline{F}_H(u_r,v_r,w_r,p,q,r)+\\ \underline{F}_K(\dot{u}_s,\dot{v}_s,\dot{w}_s,u_s,v_s,w_s,p,q,r)+\\ \underline{F}_G(f,q,y)+\\ \underline{F}_U+\\ \underline{F}_T\end{matrix} \quad (1)$$

where:

$\underline{\underline{M}}$: Mass inertia matrix.

$\dot{u}$, $\dot{v}$, $\dot{w}$, $\dot{p}$, $\dot{q}$, and $\dot{r}$: Vehicle accelerations in *X, Y, Z,* roll, pitch and yaw respectively.

$\underline{F}_d$: Vector of rigid body kinematic forces.

u, v, w, p, q, r : Vehicle velocities in *X, Y, Z,* roll, pitch and yaw respectively.

$\underline{F}_H$: Hydrodynamic force vector.

u_r, v_r, w_r : Relative velocities of the vehicle to the flow.

$\underline{F}_K$: Vector of inertial forces due to unsteady fluid motion.

$\dot{u}_s, \dot{v}_s, \dot{w}_s, u_s, v_s, w_s$: Flow accelerations and velocities.

$\underline{F}_G$: Force vector due to weight and buoyancy.

$f, q,$ and y : Orientation angles (roll, pitch and yaw).

$\underline{F}_U$: Force on the body due to the umbilical cable and chain,

$\underline{F}_T$: Vector of thruster forces.

The Hydrodynamic force vector $\underline{F}_H$ contains the hydrodynamic derivatives which need to be estimated. This paper assumes that the added mass and moments of inertia for the vehicle have already been measured or calculated.

Equation 2 gives the hydrodynamic force acting on the vehicle in the X (forwards) direction and is the first component of $\underline{F}_H$:

$$X_H = X_{qq}q^2 + X_{rr}r^2 + X_{rp}rp + X_{vr}v_r r + X_{wq}w_r q + X_{uu}u^2 + X_{vv}v_r^2 + X_{ww}w_r^2 + X_w u_r w_r \quad (2)$$

Here the relative Velocity vector is given by:

$$(u_r \quad v_r \quad w_r) = (u - u_s \quad v - v_s \quad w - w_s) \quad (3)$$

$$U = \sqrt{u_r^2 + v_r^2 + w_r^2} \quad (4)$$

Similarly in the Y (Sway) direction the hydrodynamic force is given by:

$$Y_H = Y_{p|p|}p|p| + Y_{pq}pq + Y_r u_r r + Y_p u_r p + Y_{wp}w_r p + Y_o u_r^2 + Y_v u_r v_r + Y_{v|v|}v_r|v_r| \quad (5)$$

The coefficients in front of the velocity products are the hydrodynamic derivatives or manoeuvring coefficients. For example X_{qq} describes the force in the X direction due to the square of the vehicle's pitch rate. There are similar equations and coefficients in the four remaining degrees of freedom.

III. MEASUREMENTS

Measurements taken during the ROV trial included accelerations, angular rates, loads, position and heading.

Vehicle depth, accelerations and angular rates were measured by an inertial measurement package, TOWDAS, provided by the Australian Defence Science and Technology Organisation (DSTO). TOWDAS also had a flux-gate compass for heading measurement, and a pressure sensor for depth measurement. The vehicle umbilical, thrusters, and depth control chain were strain-gauged and the position of the vehicle was measured by the High Precision Acoustic Surveying System (HPASS) developed by Curtin University's Centre for Marine Science and Technology. In this experiment HPASS was configured to use 5 acoustic transponders to provide a high level of redundancy.

All these measurements had different sampling rates and accuracies. Position fixes also experienced some drop-outs, most likely caused by parts of the vehicle obscuring the acoustic line of site between the acoustic transducer on the vehicle and one or more transponders. The frequency of drop-outs was a function of the position and orientation of the vehicle relative to the transponder web.

These measurements do not correspond directly to the vehicle state required to perform the parameter estimation. Corrections must be made for gravity effects, accelerometer alignment and bias, position fix dropouts and sampling rate differences. A Kalman filter (KF) was used to combine the measurements from the different sensors and perform the required corrections.

IV. KALMAN FILTER

A. Background

Kalman filtering is used wherever there is a need to optimally estimate the state of a system using models and observations of the system [3]. The Kalman filter takes all the available information about the current state of the system and, using the previous best state estimate, calculates the most likely current state.

The Kalman filter also has the advantage of being able to combine information from a variety of different sources, and is easily modified. It also offers the ability to deal easily (through variance assignment) with acoustic range dropouts.

Kalman filters can diverge under certain conditions. The most common explanation for this is that too much weight is placed on the dynamic model relative to the measured observations. In other words the covariance matrix becomes unrealistically small. As a result observations are ignored and inaccuracies in the model bring about divergence. Other error sources might include biases which are not compensated for, as well as roundoff and truncation errors in the calculations. [4]

Since the vehicle model and observations are non-linear, an Extended Kalman filter (EKF) was used. This filter uses a Taylor series expansion of the model and observation equations.

B. Setting Up the Filter

Three things are required in order to construct an extended Kalman filter. Firstly, the dynamic model equations are required. These equations give the vehicle state at the next time step ($t=t_{k+1}$) given the state at the previous time step ($t=t_k$). The dynamic model equations for the state estimator are:

$$\underline{R}_{k+1} = \underline{R}_k + \underline{U}_k dt + \underline{\ddot{x}}_k \frac{dt^2}{2} \quad (6)$$

$$\underline{O}_{k+1} = \underline{O}_k + C\underline{w}dt + C\underline{\dot{w}}\frac{dt^2}{2} + \underline{\ddot{x}}_k \frac{dt^3}{6} \quad (7)$$

$$\underline{U}_{k+1} = \underline{U}_k + \underline{\ddot{x}}_k dt \quad (8)$$

$$\underline{w}_{k+1} = \underline{w}_k + \underline{\dot{w}}_k dt + \underline{\ddot{x}}_k \frac{dt^2}{2} \quad (9)$$

$$\underline{\dot{w}}_{k+1} = \underline{\dot{w}}_k + \underline{\ddot{x}}_k dt \quad (10)$$

$$\underline{a}_{O\,k+1} = \underline{a}_{O\,k} + \underline{\ddot{x}}_k dt \quad (11)$$

where:
The subscripts k and $k+1$ denote the appropriate time, ie $\underline{R}_{k+1}$ is $\underline{R}$ at time t_{k+1}.

$\underline{R}$: Vehicle position vector [X Y Z].
$\underline{O}$: Orientation vector [f q y].
$\underline{U}$: Vehicle global velocity [U V W].
$\underline{w}$: Angular velocity vector [p q r].
$\dot{\underline{w}}$: Angular acceleration vector [p q r].
$\underline{a}_o$: Local vehicle acceleration vector $\begin{bmatrix}\dot{u} & \dot{v} & \dot{w}\end{bmatrix}$
$\underline{x}$: Noise vector.
dt : Amount of time between t=k+1 and t=k.
C : Transform from angular velocity/acceleration to orientation angle velocity/acceleration.

Note that these equations are relatively straight forward, and although it would be possible to use more accurate model equations this would complicate the calculation of derivatives required by the filter. The dynamic model equations given here proved to be adequate given the generally high quality of the observations.

Secondly, the observation equations need to be established. These equations give the sensor outputs that should be observed given the current state of the vehicle. The acceleration at a point $\underline{r}$ within the vehicle is given by the following:

$$\underline{a} = \underline{a}_o + \underline{w} \times (\underline{w} \times \underline{r}) + \dot{\underline{w}} \times \underline{r} - \underline{g} \qquad (12)$$

where:
$\underline{r}$: Position vector in the body-fixed axis [x y z].
$\underline{a}$: Acceleration at the position $\underline{r}$ within a rigid body.
$\underline{a}_0$: Acceleration of the origin of the coordinate system.

$$\underline{g} = \begin{bmatrix} -g \cdot \sin q \\ g \cdot \cos q \cdot \sin f \\ g \cdot \cos q \cdot \cos f \end{bmatrix}.$$

g : Acceleration due to gravity.

Equation 12 is essentially the observation equation for the accelerometers. Each accelerometer would have a different position vector, $\underline{r}$, and would be multiplied by a direction cosine to correct for the accelerometer alignment; a bias term is also added. For example the observation equation for one accelerometer would look like this:

$$measurement = \underline{a} \cdot \begin{bmatrix} l \\ m \\ n \end{bmatrix} + bias + noise \qquad (13)$$

where:
l,m,n : Accelerometer direction cosines.
$bias$: Accelerometer bias.

Angular rate observation equations are of the following form:

$$measurement = \underline{w} \cdot \begin{bmatrix} l \\ m \\ n \end{bmatrix} + bias + noise \qquad (14)$$

The observation equation for an acoustic range is as follows:

$$range = \sqrt{(X_T - X)^2 + (Y_T - Y)^2 + (Z_T - Z)^2} + noise \qquad (15)$$

where:

$[X\ Y\ Z]$: Vehicle position.
$[X_T\ Y_T\ Z_T]$: Transponder position.
$range$: Range measurement that is expected from the transponder

Thirdly, the covariance matrices of the dynamic model errors and measurement noise need to be defined. Measurement noise was characterised using stationary trials data, whereas the dynamic model covariances were estimated by simulation.

When real-time state estimates are required a forward Kalman filter must be used, but when post processing data improved results can be obtained by using a Kalman smoother (KS) which uses both past and future observations to estimate the current state. Equations for both of these cases are given in [3]. Both the KF and KS were implemented but only the KS outputs were used for parameter estimation.

Verification of the KF and KS was carried out by using a combination of simulations with and without noise, and also by comparing actual trials results with inclinometer data and other known manoeuvre details eg, manoeuvre time, circle radius.

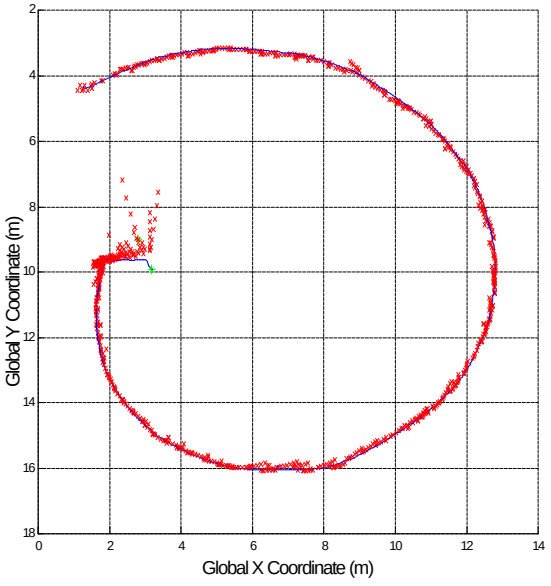

Figure 1 Plan view of position estimates for a circle manoeuvre. The vehicle started from rest at (3, 10), went straight ahead for a few seconds and then turned. Crosses are the forward Kalman filter estimates and the line is the Kalman smoother output.

V. KALMAN FILTER RESULTS

The following are some results after processing trials data with the position estimator described previously.

Figure 1 shows the filter and smoother position estimates and heading estimates for a circle manoeuvre. The initial period of acceleration can be seen on the left side of Figure 1, while the rest of the manoeuvre is also the expected circle to port. The Kalman smoother is seen to improve on the original forward filter position estimates.

At the beginning of the manoeuvre the filter has not converged and so its estimates are as much as 2 metres from the vehicle's actual position. The Kalman smoother makes a much better estimate of the initial vehicle position.

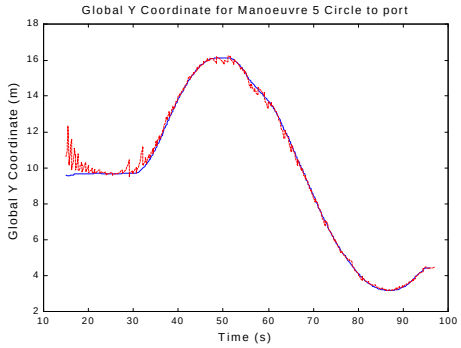

Figure 2 Global Y coordinate for circle manoeuvre to port. Forward filter and Kalman smoother estimate are shown.

Figure 2 shows that the forward filter estimates are still converging up to the 30 second mark. The mean of the differences between the smoothed and forward filter coordinate estimates for the X, Y, and Z axis, after the 30 second mark, are 5.2cm, 10.1cm and 5.5cm respectively. This shows that the Kalman smoother is making a significant correction to the forward filter estimate.

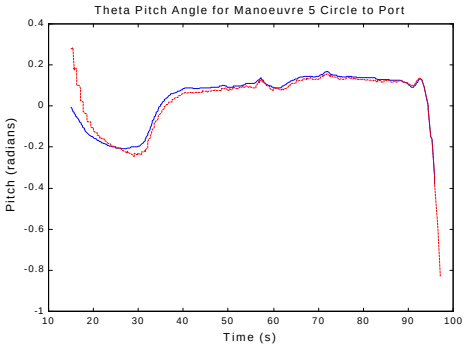

Figure 3 Vehicle pitch q for circle to port manoeuvre. Forward filter and Kalman smoother estimates are shown.

Figure 3 shows the filter and smoother estimates for the vehicle pitch during the circle manoeuvre. The initial pitch estimate of about -0.2 radians (11 degrees nose down) is in agreement with pitch inclinometer data Figure 4. Note that the vehicle state estimator does not use the pitch or roll inclinometers in its calculations and the inclinometer data is used only for validation purposes.

If the circle to port in Figure 1 was executed perfectly, the expected phase difference between global X and Y axis velocities, U and V respectively, would be 90 degrees. The first maximum positive velocity V would also be expected to occur 90 degrees before the first maximum positive U velocity. Figure 5 shows that the filter velocity estimates for U and V are approximately 90 degrees out of phase, with the peak in the Y axis velocity occurring before the X axis velocity peak as expected. The circle to port was not a perfect circle so that U and V are not perfect sine waves.

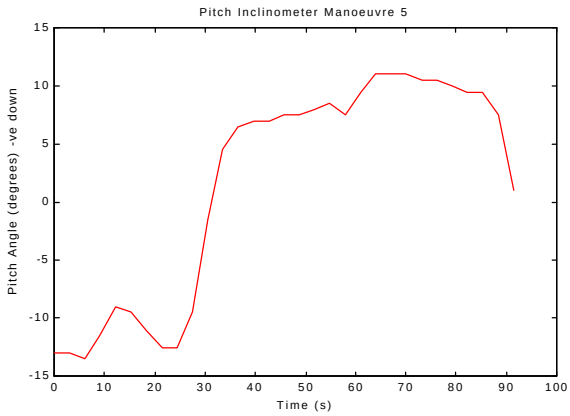

Figure 4 Data from pitch inclinometer during circle to port manoeuvre.

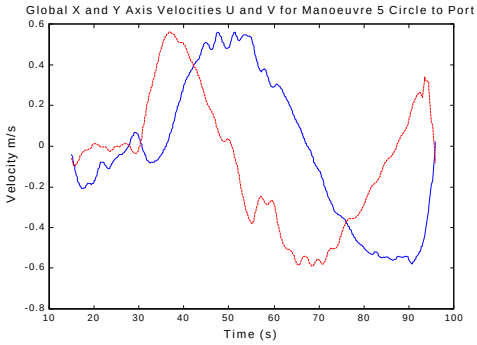

Figure 5 Global X and Y axis Velocities U and V respectively for circle to port manoeuvre. Kalman smoother estimates are shown. Solid line is the velocity U and the Dashed line is the velocity V.

The Kalman smoother estimate for $\dot{v}$ (Figure 6) has a maximum value of about 0.05ms^{-2} and a mean value of -0.002ms^{-2} between the 36 and 90 second marks (steady state circling part of circle manoeuvre). This compares well with the estimated centripetal acceleration for this manoeuvre -0.05ms^{-2} based on a vehicle velocity of 0.5ms^{-1} and a circle radius of 5m.

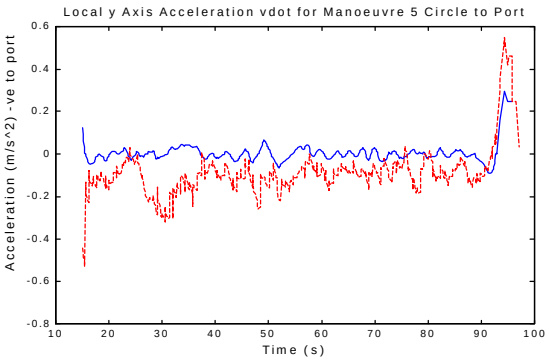

Figure 6 Acceleration along vehicle local y axis $\dot{v}$. Solid line is the Kalman smoother estimate. Dashed line is the forward filter estimate.

All vehicle state variables were estimated well enough for system identification purposes. However, the local acceleration estimates were not expected to be accurate because the accelerometer noise levels were usually greater than the accelerations being measured. Verification of the filter using simulated data showed that the filter does converge to a correct solution. Numerical calculations of the local accelerations using the estimated global velocities and vehicle orientations were also consistent with the filter's acceleration estimates.

VI. PARAMETER ESTIMATION

By rearranging Equation 1 an equation of the form $Ax=b$ can be constructed. Here x contains the hydrodynamic derivatives for one of the six degrees of freedom. b is a vector of the estimated hydrodynamic force acting on the vehicle throughout the manoeuvre, and A is a matrix containing velocity products with each row corresponding to one time step.

When least squares was applied to this model it was evident that the residuals were correlated and hence either the disturbances were not independent or there was a deficiency in the hydrodynamic model. Investigation of this correlation showed that the correlation was due primarily to the umbilical and chain forces.

In order to correctly apply least squares it was necessary to model the correlation with a first order autoregressive process $z_n=e_n+fz_{n-1}$. Here z_n is the residual at time n and e_n is white noise. This produces the non linear least squares problem given by Equation 16.

$$b_n = fb_{n-1} + A_n x - fA_{n-1}x \qquad (16)$$

A Gauss-Newton algorithm was used to solve for the model parameters, and a stepwise regression algorithm was used to select the hydrodynamic derivatives that were included in the final model for each manoeuvre.

The following set of six tables (tables 1 to 6) show the estimated hydrodynamic coefficients for three of the trials manoeuvres, along with the coefficients as measured on a 1/3 scale model of the PAP-104 by a planar motion mechanism (PMM). PMM coefficients not shown were not measured.

Trials results with an asterix have the higher significance (f-test value) in describing the hydrodynamic force for the relevant degree of freedom during the specified manoeuvre. Blank spaces are coefficients not chosen to describe the manoeuvre on the basis of significance tests. The percentage figures are the approximate standard errors of the estimated coefficients as a percentage of the corresponding coefficient.

$Y_{v|v|}'$ is within experimental error of the PMM measurement, and X_{uu}' has the same order of magnitude as the PMM measurement. Of the six coefficients that are identified in more than one manoeuvre Y_{pq}, Z_{uq}, and $K'_{v(v^2+w^2)^{0.5}}$ are not within error of one another. Two of the three Z_{uq} measurements are within error of each other.

Considering the number of error sources in the trials data and the conditions the UUV was operating under the results are reasonable.

	Circle		Zigzag		Line		PMM	
X_{uu}'	-0.076 *	40%					-0.012	4.2%
X_{uw}'			0.61 *	19%				
X_{vv}'			0.57 *	21%			0.043	3.9%
X_{vr}'					3.79	64%		
X_{ww}'	-1.5	35%						
X_{wq}'	-4.75	33%	-2.5	29%				
X_{rr}'	-0.82 *	27%						

Table 1 PAP-104 non-dimensional x-axis surge coefficients

	Circle		Zigzag		Line		PMM	
Y_{uu}'	0.061	44%						
Y_{up}'	-0.39	26%						
Y_{ur}'	0.89 *	9%					0.04	93%
$Y_{v\|v\|}'$	-0.90	50%					-0.30	4.3%
Y_{wp}'					3.7	39%		
$Y_{p\|p\|}'$			-1.8 *	29%				
Y_{pq}'	-5.4	41%	-1.9	37%				

Table 2 PAP-104 non-dimensional y-axis sway coefficients

	Circle		Zigzag		Line	
Z_{uq}'	-0.77	22%	0.26	45%	-0.38	68%
Z_{uw}'			-0.18	41%		

Table 3 PAP-104 non-dimensional z-axis heave coefficients

	Circle		Zigzag		Line	
K_{up}'			0.09	33%		
$K'_{v(v^2+w^2)^{0.5}}$	0.42 *	27%			0.09	15%
K_{vq}'					0.39	17%
K_{wr}'	0.33	31%				
K_{pq}'			0.86 *	32%		

Table 4 PAP-104 non-dimensional roll coefficients

	Circle		Zigzag		Line		PMM	
M_{uu}'			-0.10	19%			-0.002	12 %
M_{uq}'	-0.86 *	19%	-0.72 *	14%				
M_{uw}'	-0.25	28%						
M_{vv}'	0.94	47%					-0.013	18%
M_{vp}'	-2.5	27%						
M_{vr}'	2.1 *	23%			3.4	33%		
$M'_{w^3/U}$			2.2	27%				
M_{rr}'	-0.48	35%						

Table 5 PAP-104 non-dimensional pitch coefficients

	Circle		Zigzag		Line		PMM	
N_{uu}'			-0.04	42%				
N_{up}'	0.32	22%						
N_{ur}'	-0.54 *	8%					-0.02	28 %
N_{vw}'					-0.07	26%		
N_{qr}'			0.69 *	29%				

Table 6 PAP-104 non-dimensional yaw coefficients

VII. CONCLUSIONS

An extended Kalman smoother was used to reconstruct system identification trials manoeuvres. The vehicle state estimator was validated using a 6DOF UUV model and reconstructed trials manoeuvre data were self consistent.

Identification of the hydrodynamic coefficients was carried out using a stepwise regression algorithm. It was necessary to remove correlation in the data using a first order autoregressive model in order to apply least squares correctly, and thus obtain better hydrodynamic coefficient estimates.

There were significant differences between some of the hydrodynamic coefficients obtained using system identification and those measured using the planar motion mechanism. The coefficients obtained using SI also had larger standard errors associated with them than the PMM measurements.

Possible reasons for the discrepancies between the two sets of coefficients include measurement errors in the thruster, umbilical and chain force measurements, the difficulty of performing manoeuvres that would adequately excite the coefficients with a two-thruster vehicle, and the fact that the SI trials gave effective hydrodynamic coefficients for a complete, operational vehicle whereas the PMM measurements were made on a model of the shell of the vehicle without thrusters.

A direct comparison between PMM and SI trials coefficients does not reveal much about the effect of these different values on vehicle performance. A better comparison would be to compare the performance of vehicles simulated with the two sets of coefficients in a series of simulated trials manoeuvres. This work is ongoing.

ACKNOWLEDGEMENTS

This work was funded by the Australian Maritime Engineering CRC. Further assistance was provided by the Centre for Marine Science and Technology and the Defence Science and Technology Organisation (DSTO

REFERENCES

1. Anderson. B. Personal Communication 1997.

2. Bradbury, T.C. "*Theoretical Mechanics*" John Wiley & Sons, 1968.

3. Chui, C.K. & Chen, G. "*Kalman Filtering with Real-Time Applications 2nd Edition*", Springer-Verlag, 1991.

4. Fitzgerald, R.J, "*Divergence of the Kalman Filter*", IEEE Trans. Automat. Contr., vol AC-16, Dec 1971, pp.736-747.